



Article

Crack Length Effect on the Fracture Behavior of Single-Crystals and Bi-Crystals of Aluminum

Wilmer Velilla-Díaz ^{1,2,*} and Habib R. Zambrano ^{3,*} ¹ Departamento de Ingeniería Mecánica, Universidad Autónoma del Caribe, Barranquilla 080020, Colombia² Instituto de Diseño y Métodos Industriales, Universidad Austral de Chile, Valdivia 5110566, Chile³ Departamento de Ingeniería Mecánica, Universidad del Norte, Barranquilla 081007, Colombia

* Correspondence: wilmer.velilla@uac.edu.co (W.V.-D.); hzambrano@uinorte.edu.co (H.R.Z.);

Tel.: +57-301-371-3776 (W.V.-D.)

Abstract: Molecular dynamics simulations of cracked nanocrystals of aluminum were performed in order to investigate the crack length and grain boundary effects. Atomistic models of single-crystals and bi-crystals were built considering 11 different crack lengths. Novel approaches based on fracture mechanics concepts were proposed to predict the crack length effect on single-crystals and bi-crystals. The results showed that the effect of the grain boundary on the fracture resistance was beneficial increasing the fracture toughness almost four times for bi-crystals.

Keywords: fracture toughness; crack length effect; grain boundary; bi-crystals; single-crystals; molecular dynamics simulations



Citation: Velilla-Díaz, W.; Zambrano, H.R. Crack Length Effect on the Fracture Behavior of Single-Crystals and Bi-Crystals of Aluminum. *Nanomaterials* **2021**, *11*, 2783. <https://doi.org/10.3390/nano11112783>

Academic Editor: Cinzia Sada

Received: 17 September 2021

Accepted: 12 October 2021

Published: 21 October 2021

Publisher's Note: MDPI stays neutral with regard to jurisdictional claims in published maps and institutional affiliations.



Copyright: © 2021 by the authors. Licensee MDPI, Basel, Switzerland. This article is an open access article distributed under the terms and conditions of the Creative Commons Attribution (CC BY) license (<https://creativecommons.org/licenses/by/4.0/>).

1. Introduction

Recently, the development of atomistic models based on molecular dynamics simulations made possible to investigate the mechanical behavior of nanocrystals for a few materials, such as aluminum (Al) [1–7]. The first analyses were performed to investigate tensile mechanical properties, viz., ultimate tensile strength (S_U) and young's module (E) [8–13]. Later, in order to study the fracture behavior, atomistic simulations of nanocrystals that considered small defects, such as cracks and voids, were developed [14–21]. Based on cracked nanocrystal simulations, it was possible to estimate fracture mechanics properties for some nanocrystal materials. To obtain fracture mechanics properties, such as fracture toughness different fracture mechanics parameter were used to analyze results from molecular dynamics simulations of cracked nanocrystals [22–29]. In addition, some researchers tested the suitability of the fracture mechanics parameters to predict the fracture of nanocrystals [30]. Regarding the fracture behavior of materials at the macroscale, one challenge in fracture mechanics was to obtain an accurate model to describe the effect of the crack length on the fracture of the components. The experiments carried out by different authors (at the macroscale) demonstrated that when a crack was long enough fracture mechanics parameters, such as stress intensity factor (K), J -integral (J), and crack tip opening displacement ($CTOD$) were suitable to predict the fracture of cracked components, thus the stress at the fracture (σ_U) was defined by the fracture toughness [31] (Figure 1). However, the experiments showed that σ_U increased rapidly as the initial crack length was smaller, but when the crack was vanishing σ_U tended to a fixed value which was S_U [32] (Figure 1). In order to establish when the crack was long and when it was too small, in other words, when σ_U was predicted by the fracture toughness and when it was by the S_U , the characteristic crack length (l_0) was defined. Crack lengths much larger than l_0 were long cracks and σ_U was governed by the fracture toughness, but crack lengths much smaller than l_0 were small cracks and the σ_U was defined by S_U . This crack length effect was extensively investigated at the macroscale by Taylor [32]. A schematic representation of the crack length effect was showed (Figure 1). However, the crack length

effect was firstly studied for fatigue failure by Kitagawa et al. [33] and El Haddad et al. [34]. Kitagawa and Takahashi were the first researchers in defining the crack length effect by means of a diagram (Figure 1), but it was applied for fatigue failure analysis of cracked components [33]. In order to analyze the crack length effect in fatigue, El Haddad proposed to modify the stress intensity factor range by adding (to the actual crack length) a constant length that depended on the material properties [34]. Modifying slightly the crack length to calculate the stress intensity factor range, El Haddad obtained an equation that tended to a fixed value (fatigue limit) when the actual crack length was very small, and it led to the usual stress intensity factor range when the crack length was long enough. The El Haddad fatigue model reproduced the Kitagawa-Takahashi diagram [33]. The same concept was adopted and extended to quasi-static monotonic loading failure analysis of components by Taylor in the theory of critical distances [32]. The present investigation was an attempt to extend the same concept into the nanoscale, therefore molecular dynamics simulations of cracked nanocrystals of Al with a wide range of crack lengths were performed in order to study the crack length effect in single-crystals and bi-crystals of Al. The results showed the crack length effect similar to that described above in the cracked nanocrystals. In order to predict the crack length effect on nanocrystals two models were proposed. First, linear elastic fracture mechanics (LEFM) concepts were used to develop an approach to predict σ_U based on K . Second, due to the lack of accuracy of the LEFM model, an elastic-plastic fracture mechanics (EPFM) model was proposed. A novel equation to estimate l_0 for nanocrystals was formulated. Finally, the effect of the grain boundary on the fracture behavior was also investigated.

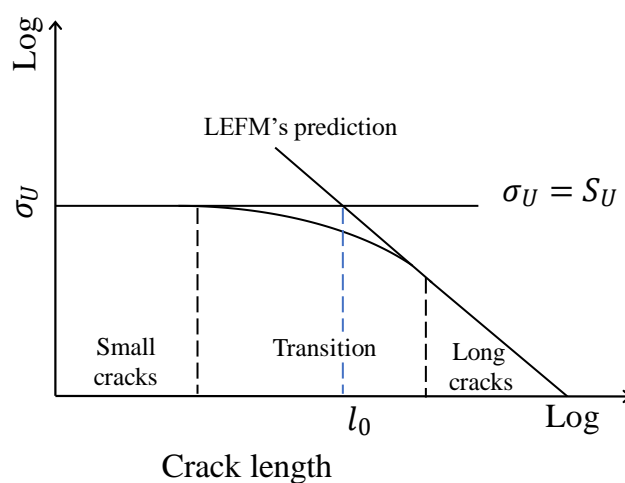


Figure 1. Schematic representation of the crack length effect.

2. Methodology

2.1. Modeling

The molecular dynamics simulations were performed in the code LAMMPS [35]. The atomistic system was first equilibrated using the conjugate gradient method at a pressure of 1.01 bar and at temperature of 300 K using the isobaric-isothermal ensemble (NPT) for 20,000 timesteps of 0.001 ps. The Nose-Hoover barostat and thermostat were implemented to sustain the pressure and temperature. Once the system was equilibrated, loops of deformation-equilibrium were performed until the global stress was close to zero indicating the crystal fracture. Each deformation increment was 0.01% in z-direction with a strain rate of 1×10^{-4} /ps. The length of the atomistic system in the z-direction kept constant during the equilibrium process. The deformation-equilibrium loops were performed using the NPT ensemble applying 10,000 and 20,000 timesteps for deformation and equilibrium, respectively. The embedded atom method potential from Mendeleev et al. [36] was implemented, which have been used by other researchers in molecular dynamics simulations of cracked nanocrystals of Al [37,38]. The simulation boxes of the cracked

single-crystals and bi-crystals were represented in Figure 2a,b. The dimensions of the simulation boxes were $60a \times 20a \times 40a$ ($24.3 \times 8.1 \times 16.2 \text{ nm}^3$) for both single-crystal and bi-crystal, where the lattice parameter for Al was $a = 0.405 \text{ nm}$. To analyze the effect of the grain boundary, a misorientation grain boundary with tilted angle of 30° was considered in bi-crystal simulations. The crack height was $2.5a$ for all specimens, and the initial crack lengths were $l_i = 1a, 2a, 3a, 5a, 10a, 15a, 20a, 30a, 40a, 50a, 55a$. The atomistic systems contained approximately 195,000 particles each one. The virial stress tensor was used to compute the global stress [39]. The stress-strain curves obtained from the simulations were presented in Figures 3 and 4 with the corresponding initial crack length l_i for single-crystals and bi-crystals, respectively. The volume of the atoms were computed using the Voronoi tessellation in voro++ [40]. DXA [41] was used for dislocation analysis in OVITO [42].

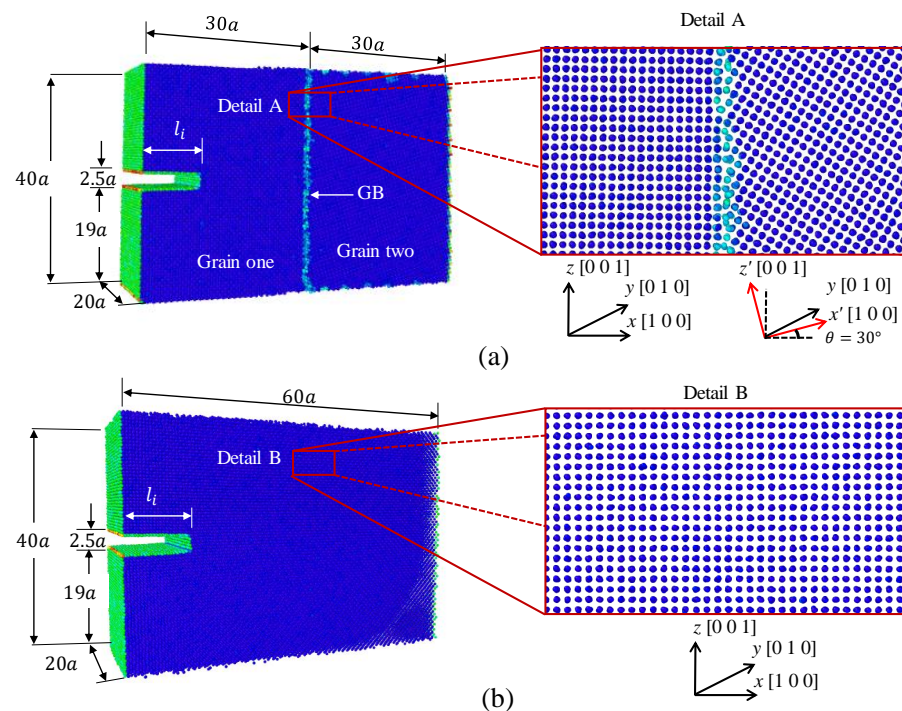


Figure 2. Atomistic system for (a) bi-crystal and (b) single-crystal Al.

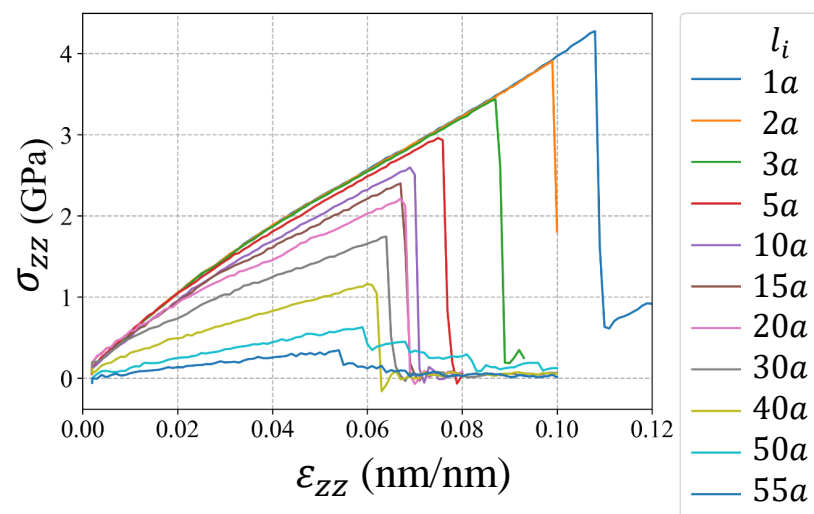


Figure 3. Simulation results of tensile tests for single-crystals Al with different l_i .

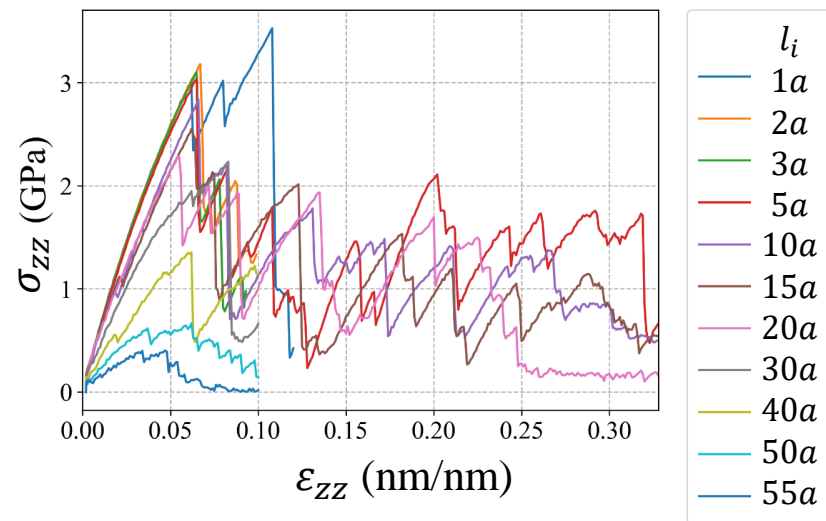


Figure 4. Simulation results of tensile tests for bi-crystals Al with different l_i .

2.2. Characteristic Crack Length

The same effective crack length ($l_0 + l_i$) proposed by El Haddad [34] to evaluate the crack length effect on the fatigue limit of cracked components was used to estimate the stress intensity factor in mode I (K_I) for cracked nanocrystals of Al:

$$K_I = f \cdot \sigma_{zz} \cdot \sqrt{\pi \cdot (l_0 + l_i)} \quad (1)$$

where σ_{zz} was assumed to be the global stress (calculated based on the virial stress tensor) in the z -direction and f was the geometric factor for edge cracks given by [43]:

$$f = 0.265(1 - \alpha)^4 + \frac{0.857 + 0.265\alpha}{(1 - \alpha)^{3/2}} \quad (2)$$

where $\alpha = (l_0 + l_i)/60a$. As established in a previous investigation [44], the fracture mechanics parameter J was found to be accurate to predict the effect of cracks on single-crystals and bi-crystals. In the same research work different approaches were successfully used for estimating J from molecular dynamics simulations. Therefore, in order to use J , in this investigation, Equation (1) was rewritten as a function of J . To obtain an equivalent expression for Equation (1) in terms of J , K_I was replaced by $K_I = \sqrt{(J \cdot E')}$ [43], and the following equation was obtained:

$$J = \frac{f^2 \cdot \sigma_{zz}^2 \cdot \pi \cdot (l_0 + l_i)}{E'} \quad (3)$$

where l_0 was possible to determine assuming the limiting conditions for a cracked nanocrystal with a vanishing crack length undergoing σ_U , viz., when $l_i \rightarrow 0$ and $\sigma_{zz} = \sigma_U$, thus $\sigma_U = S_U$ and $J = J_C$ (where J_C was the fracture toughness), thus:

$$l_0 = \frac{J_C \cdot E'}{f^2 \cdot S_U^2 \cdot \pi} \quad (4)$$

where $E' = E/(1 - \nu^2)$ for plane strain and $E' = E$ for plane stress [43], and ν was the Poisson's ratio. Equation (4) showed more explicitly the dependency of l_0 on the stress state at the crack tip (plane strain or plane stress), which was not evident in the classical formulation proposed by El Haddad [34] for fatigue failure and extended to quasi-static monotonic loading failure by Taylor [32].

2.3. Fracture Prediction

An expression for predicting the crack length effect on σ_U was obtained by replacing J by J_C and σ_{zz} by $\bar{\sigma}_U$ in Equation (3), and solving the equation for $\bar{\sigma}_U$, hence:

$$\bar{\sigma}_U = \sqrt{\frac{J_C \cdot E'}{f^2 \cdot \pi \cdot (l_0 + l_i)}} \quad (5)$$

where $\bar{\sigma}_U$ was the predicted fracture stress. The predictions of Equation (5) were compared with σ_U in Section 3 for single-crystals and bi-crystals, where σ_U was obtained from molecular dynamics simulations by computing the virial stress tensor as mentioned in Section 2.1. However, in order to generate an alternative and more accurate methodology to predict the crack length effect, the EPFM was used by means of the parameter $CTOD$. Therefore, the $CTOD$ was estimated at the fracture ($CTOD_U$) from the simulations and used to calculate an equivalent fracture stress (σ_{Ueq}). In order to obtain σ_{Ueq} , J was obtained from $CTOD_U(J_{CTOD})$ as [31]:

$$J_{CTOD} = \frac{\sigma_U \cdot CTOD_U \cdot \pi}{4} \quad (6)$$

where $CTOD_U$ was assumed to be the distance between two selected atoms at the crack tip just before the fracture as proposed in [44–47]. Figure 5 showed how the $CTOD$ was estimated from the simulations. Finally, σ_{Ueq} was obtained assuming $l_0 = 0$, and replacing J by J_{CTOD} and σ_{zz} by σ_{Ueq} in Equation (3), thus:

$$\sigma_{Ueq} = \sqrt{\frac{J_{CTOD} \cdot E'}{f^2 \cdot \pi \cdot l_i}} \quad (7)$$

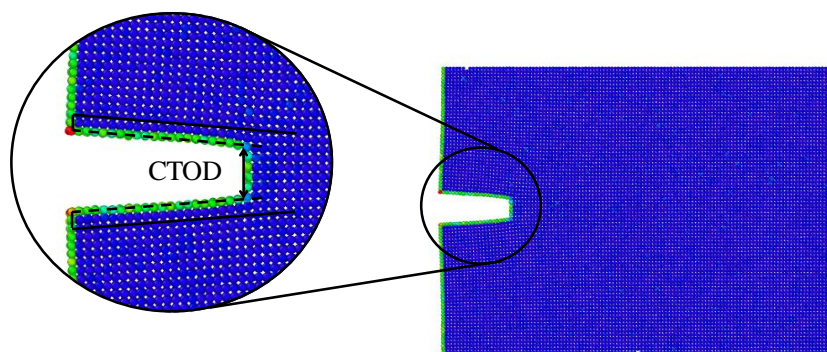


Figure 5. $CTOD$ estimation.

3. Results and Discussion

J_{CTOD} and σ_{Ueq} were estimated by means of Equations (6) and (7), respectively, for plane strain, and the results summarized in Table 1. σ_U and $CTOD_U$ were obtained from the simulations and also reported in Table 1. Due to the fact that the fracture toughness was the material property suitable to predict σ_U for long cracks ($l_i > l_0$), therefore J_C was obtained by fitting Equation (5) to the results obtained from the molecular dynamics simulations for Al crystals with $l_i > l_0$ (Figure 6a,b). To fit Equation (5) the least squares method was implemented, and the respective J_C that minimized the error was reported in Table 2 for single-crystals and bi-crystals. On one hand, Figure 6a,b evidenced that the obtained accuracy was poor, indicating that using only the virial stress tensor to analyze the crack length effect was not suitable. However, Equation (5) was appropriated to reproduce the trend of the results to reach a fixed value (S_U) when the crack length was vanishing. On the other hand, Figure 7a,b showed that using the EPFM's parameter $CTOD$ for estimating σ_{Ueq} by means of Equations (6) and (7) led to an accurate methodology obtaining consistent

estimations for J_C , where J_C was obtained by fitting Equation (5) to the results from long cracks (Figure 7a,b). The J_C that minimized the error in Figure 7a,b were presented in Table 3 for single-crystals and bi-crystals. Using this EPFM methodology, the obtained J_C coincided with the value reported in [44] for single-crystals. Regarding J_C for bi-crystals, the results in Figure 7b indicated two different fracture behaviors. One for crack lengths larger than the selected grain size ($l_i \geq 30a$) and other for crack lengths smaller than the grain size ($l_i < 30a$). Such a behavior was not unexpected, because the grain boundary showed significant effect on the fracture behavior of bi-crystals, while the crack tip was behind the grain boundary ($l_i < 30a$). However, when the crack tip was beyond the grain boundary ($l_i \geq 30a$) the effect on the fracture behavior was irrelevant. In order to investigate the effect of the grain boundary on the fracture behavior, Equation (5) was fitted twice for analyzing bi-crystals. First for bi-crystals with $l_i \geq 30a$ and second for $l_i < 30a$, as shown in Figure 7b, and the results were reported in Table 3. The obtained S_U and J_C for bi-crystals with $l_i \geq 30a$ were almost the same values obtained for single-crystals, therefore the adjusted curves coincided for single-crystals and bi-crystals with $l_i \geq 30a$ (Figure 7a,b). The results for bi-crystals showed a substantial drop of 52% and 73% in S_U and J_C , respectively, when the crack length exceeded the grain size indicating that the grain boundary effect was beneficial for the fracture resistance, while the boundary was behind the crack tip. The S_U obtained for bi-crystals with $l_i < 30a$ matched the value reported in [48].

Table 1. Data used for estimating $\bar{\sigma}_U$ and J_C .

Specimen	l_i (m)	σ_U (GPa)	$CTOD_U$ (m)	J_{CTOD} (J/m ²)	σ_{Ueq} (GPa)
Single-crystal	4.050×10^{-10}	4.2700	1.349×10^{-9}	0.3637	3.9434
	8.100×10^{-10}	3.9098	1.247×10^{-9}	0.6161	3.5934
	1.215×10^{-9}	3.4300	1.256×10^{-9}	3.3830	6.7960
	2.025×10^{-9}	2.9600	1.370×10^{-9}	3.1852	4.9659
	4.050×10^{-9}	2.5600	1.407×10^{-9}	2.8297	2.9978
	6.075×10^{-9}	2.3800	1.396×10^{-9}	2.6093	2.0493
	8.100×10^{-9}	2.1300	1.428×10^{-9}	2.3889	1.4288
	1.215×10^{-8}	1.7436	1.333×10^{-9}	1.8252	0.6480
	1.620×10^{-8}	1.1619	1.222×10^{-9}	1.1147	0.2297
	2.025×10^{-8}	0.6291	1.720×10^{-9}	0.8497	0.0609
	2.228×10^{-8}	0.3432	1.222×10^{-9}	0.3293	0.0125
	Bi-crystal	4.050×10^{-10}	3.5200	-	-
8.100×10^{-10}		3.1800	-	-	-
1.215×10^{-9}		3.1000	-	-	-
2.025×10^{-9}		3.0400	5.869×10^{-9}	14.0130	10.4158
4.050×10^{-9}		2.8400	5.623×10^{-9}	12.5421	6.3113
6.075×10^{-9}		2.5500	6.222×10^{-9}	12.4602	4.4782
8.100×10^{-9}		2.2800	6.063×10^{-9}	10.8568	3.0459
1.215×10^{-8}		2.2318	2.237×10^{-9}	3.9204	0.9497
1.620×10^{-8}		1.3525	2.395×10^{-9}	2.5440	0.3471
2.025×10^{-8}		0.6654	2.174×10^{-9}	1.1362	0.0704
2.228×10^{-8}		0.4012	1.723×10^{-9}	0.5429	0.0161

Table 2. Fracture toughness estimation based on virial stress tensor.

	l_0 (m)	J_C (J/m ²)	S_U (GPa)	Error
Single-crystal	5.97×10^{-10}	1.33	6.18	5.6337
Bi-crystal	3.45×10^{-9}	9.61	6.18	1.6812

Table 3. Fracture toughness estimation based on *CTOD*.

	l_0 (m)	J_C (J/m ²)	S_U (GPa)	Error
Single-crystal	1.35×10^{-9}	3.15	6.18	0.2400
Bi-crystal $l_i < 30a$	1.31×10^{-9}	13.25	12.92	0.2348
Bi-crystal $l_i \geq 30a$	1.53×10^{-9}	3.60	6.18	0.0095

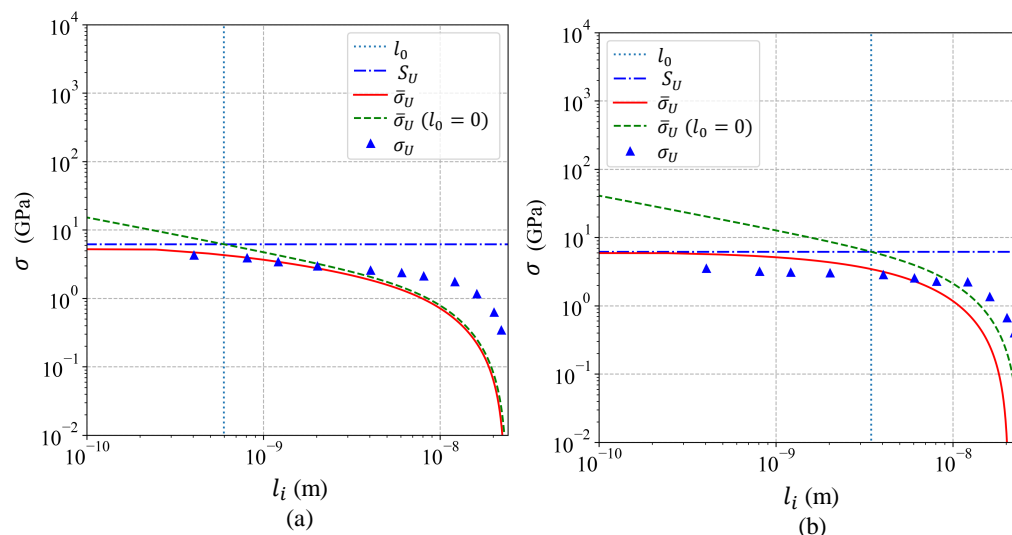


Figure 6. Model based on the LEFM parameter K_I and virial stress tensor (a) for single-crystals Al and (b) for bi-crystals Al.

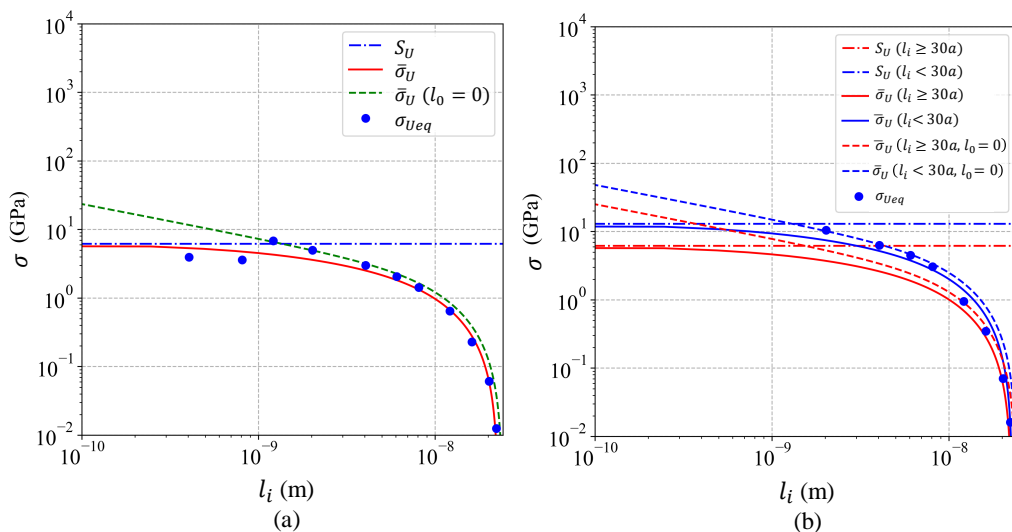


Figure 7. Model based on the EPFM parameter *CTOD* (a) for single-crystals Al and (b) for bi-crystals Al.

4. Conclusions

Based on molecular dynamics simulations, the effect of the crack length was evidenced and investigated on single-crystals and bi-crystals of Al. In addition, the effect of the grain boundary on the fracture behavior was analyzed. The following conclusions were drawn:

- The proposed approach based on the LEFM parameter K_I and the virial stress tensor was not appropriate to describe the crack length effect, as shown in Figure 6a,b;
- The proposed approach based on the EPFM parameter *CTOD* demonstrated to be accurate to predict the crack length effect in single-crystals and bi-crystals, as evidenced in Figure 7a,b;

- The effect of the grain boundary was beneficial increasing the fracture resistance, viz., S_U and J_C , as demonstrated Figure 7b.

Author Contributions: Conceptualization, W.V.-D. and H.R.Z.; Formal analysis, H.R.Z.; Investigation, W.V.-D.; Methodology, H.R.Z.; Project administration, W.V.-D.; Resources, H.R.Z.; Writing—original draft, W.V.-D.; Writing—review and editing, H.R.Z. and W.V.-D. All authors have read and agreed to the published version of the manuscript.

Funding: This research was funded by Universidad del Norte.

Institutional Review Board Statement: Not applicable.

Informed Consent Statement: Not applicable.

Data Availability Statement: Data is contained within the present article.

Conflicts of Interest: The authors declare no conflict of interest.

References

- Chandra, S.; Kumar, N.N.; Samal, M.K.; Chavan, V.M.; Raghunathan, S. An atomistic insight into the fracture behavior of bicrystal aluminum containing twist grain boundaries. *Comput. Mater. Sci.* **2017**, *130*, 268–281. [[CrossRef](#)]
- Chandra, S.; Samal, M.K.; Chavan, V.M.; Patel, R.J. An atomistic study of resistance offered by twist grain boundaries to incoming edge dislocation in FCC metals. *Mater. Lett.* **2016**, *180*, 11–14. [[CrossRef](#)]
- Stepanova, L.; Bronnikov, S. A computational study of the mixed-mode crack behavior by molecular dynamics method and the multi—Parameter crack field description of classical fracture mechanics. *Theor. Appl. Fract. Mech.* **2020**, *109*, 102691. [[CrossRef](#)]
- Yamakov, V.; Wolf, D.; Phillpot, S.R.; Mukherjee, A.K.; Gleiter, H. Deformation-mechanism map for nanocrystalline metals by molecular-dynamics simulation. *Nat. Mater.* **2004**, *3*, 43–47. [[CrossRef](#)]
- Chandra, S.; Samal, M.K.; Chavan, V.M.; Patel, R.J. Atomistic simulations of interaction of edge dislocation with twist grain boundaries in Al-effect of temperature and boundary misorientation. *Mater. Sci. Eng. A* **2015**, *646*, 25–32. [[CrossRef](#)]
- Akbarian, S.; Deghani, K. On the molecular dynamics simulation of fatigue behavior of pre-cracked aluminum chip for NEMS application: Effect of cyclic loading mode and surface roughness geometry. *Int. J. Fatigue* **2020**, *135*, 105570. [[CrossRef](#)]
- Subedi, S.; Handrigan, S.M.; Morrissey, L.S.; Nakhla, S. Mechanical properties of nanocrystalline aluminium: A molecular dynamics investigation. *Mol. Simul.* **2020**, *46*, 898–904. [[CrossRef](#)]
- DeCelis, B.; Argon, A.S.; Yip, S. Molecular dynamics simulation of crack tip processes in alpha-iron and copper. *J. Appl. Phys.* **1983**, *54*, 4864–4878. [[CrossRef](#)]
- Cheung, K.S.; Yip, S. A molecular-dynamics simulation of crack-tip extension: The brittle-to-ductile transition. *Model. Simul. Mater. Sci. Eng.* **1994**, *2*, 865–892. [[CrossRef](#)]
- Swadener, J.G.; Baskes, M.I.; Nastasi, M. Molecular Dynamics Simulation of Brittle Fracture in Silicon. *Phys. Rev. Lett.* **2002**, *89*, 085503. [[CrossRef](#)] [[PubMed](#)]
- Schiotz, J.; Jacobsen, K.W. A Maximum in the Strength of Nanocrystalline Copper. *Science* **2003**, *301*, 1357–1359. [[CrossRef](#)] [[PubMed](#)]
- Falk, M.L.; Langer, J.S. Dynamics of viscoplastic deformation in amorphous solids. *Phys. Rev. E Stat. Phys. Plasmas Fluids Relat. Interdiscip. Top.* **1998**, *57*, 7192–7205. [[CrossRef](#)]
- Van Swygenhoven, H.; Spaczér, M.; Caro, A. Role of low and high angle grain boundaries in the deformation mechanism of nanophase Ni: A molecular dynamics computer simulation study. *Nanostructured Mater.* **1998**, *10*, 819–828. [[CrossRef](#)]
- Cheung, K.S.; Yip, S. Brittle-Ductile Transition in Intrinsic Fracture Behavior of Crystals Kin. *Phys. Rev. Lett.* **1990**, *65*, 2804–2807. [[CrossRef](#)] [[PubMed](#)]
- Karimi, M.; Roarty, T.; Kaplan, T. Molecular dynamics simulations of crack propagation in Ni with defects. *Model. Simul. Mater. Sci. Eng.* **2006**, *14*, 1409–1420. [[CrossRef](#)]
- Buehler, M.J.; Yao, H.; Gao, H.; Ji, B. Cracking and adhesion at small scales: Atomistic and continuum studies of flaw tolerant nanostructures. *Model. Simul. Mater. Sci. Eng.* **2006**, *799*, 799–816. [[CrossRef](#)]
- Potirniche, G.; Horstemeyer, M.; Gullett, P.; Jelinek, B. Atomistic modelling of fatigue crack growth and dislocation structuring in FCC crystals. *Proc. R. Soc. A Math. Phys. Eng. Sci.* **2006**, *462*, 3707–3731. [[CrossRef](#)]
- Farkas, D.; Van Petegem, S.; Derlet, P.M.; Van Swygenhoven, H. Dislocation activity and nano-void formation near crack tips in nanocrystalline Ni. *Acta Mater.* **2005**, *53*, 3115–3123. [[CrossRef](#)]
- Ma, L.; Xiao, S.; Deng, H.; Hu, W. Molecular dynamics simulation of fatigue crack propagation in bcc iron under cyclic loading. *Int. J. Fatigue* **2014**, *68*, 253–259. [[CrossRef](#)]
- Kedharnath, A.; Panwar, A.S.; Kapoor, R. Molecular dynamics simulation of the interaction of a nano-scale crack with grain boundaries in α -Fe. *Comput. Mater. Sci.* **2017**, *137*, 85–99. [[CrossRef](#)]
- Chakraborty, S.; Zhang, J.; Ghosh, S. Accelerated molecular dynamics simulations for characterizing plastic deformation in crystalline materials with cracks. *Comput. Mater. Sci.* **2016**, *121*, 23–34. [[CrossRef](#)]

22. Petucci, J.; Leblond, C.; Karimi, M. Molecular dynamics simulations of brittle fracture in fcc crystalline materials in the presence of defects. *Comput. Mater. Sci.* **2014**, *86*, 130–139. [[CrossRef](#)]
23. Jones, R.E.; Zimmerman, J.A. The construction and application of an atomistic J-integral via Hardy estimates of continuum fields. *J. Mech. Phys. Solids* **2010**, *58*, 1318–1337. [[CrossRef](#)]
24. Xu, G.Q.; Demkowicz, M.J. Computing critical energy release rates for fracture in atomistic simulations. *Comput. Mater. Sci.* **2020**, *181*, 109738. [[CrossRef](#)]
25. Zhuo, X.R.; Kim, J.H.; Beom, H.G. R -curve Evaluation of Copper and Nickel Single Crystals Using Atomistic Simulations. *Crystals* **2018**, *8*, 441. [[CrossRef](#)]
26. Jones, R.E.; Zimmerman, J.A.; Oswald, J.; Belytschko, T. An atomistic J-integral at finite temperature based on Hardy estimates of continuum fields. *J. Phys. Condens. Matter* **2011**, *23*, 015002. [[CrossRef](#)]
27. Ferdous, S.F.; Adnan, A. Mode-I Fracture Toughness Prediction of Diamond at the Nanoscale. *J. Nanomech. Micromech.* **2017**, *7*, 04017010. [[CrossRef](#)]
28. Brochard, L.; Tejada, I.G.; Sab, K. From yield to fracture, failure initiation captured by molecular simulation. *J. Mech. Phys. Solids* **2016**, *95*, 632–646. [[CrossRef](#)]
29. Lee, G.H.; Beom, H.G. Mixed-mode fracture toughness testing of a Cu/Ag bimetallic interface via atomistic simulations. *Comput. Mater. Sci.* **2020**, *183*, 109806. [[CrossRef](#)]
30. Velilla-Díaz, W.; Ricardo, L.; Palencia, A.; Zambrano, H.R. Fracture toughness estimation of single-crystal aluminum at nanoscale. *Nanomaterials* **2021**, *11*, 680. [[CrossRef](#)] [[PubMed](#)]
31. Anderson, T.L. *Fracture Mechanics*, 3rd ed.; Taylor & Francis: Oxfordshire, UK, 2005.
32. Taylor, D. *The Theory of Critical Distances: A New Perspective in Fracture Mechanics*; Elsevier: Oxford, UK, 2007. [[CrossRef](#)]
33. Kitagawa, H.; Takahashi, S. Applicability of fracture mechanics to very small cracks or the cracks in early stage. In Proceedings of the Second International Conference on the Mechanical Behaviour of Materials, Cleveland, OH, USA, 16–20 August 1976; pp. 627–631.
34. El Haddad, M.H.; Smith, K.N.; Topper, T.H. Fatigue Crack Propagation of Short Cracks. *J. Eng. Mater. Technol.* **1979**, *101*, 42–46. [[CrossRef](#)]
35. Plimpton, S. Fast Parallel Algorithms for Short—Range Molecular Dynamics. *J. Comput. Phys.* **1995**, *117*, 1–19. [[CrossRef](#)]
36. Mendeleev, M.I.; Kramer, M.J.; Becker, C.A.; Asta, M. Analysis of semi-empirical interatomic potentials appropriate for simulation of crystalline and liquid Al and Cu. *Philos. Mag.* **2008**, *88*, 1723–1750. [[CrossRef](#)]
37. Horstemeyer, M.F.; Farkas, D.; Kim, S.; Tang, T.; Potirniche, G. Nanostructurally small cracks (NSC): A review on atomistic modeling of fatigue. *Int. J. Fatigue* **2010**, *32*, 1473–1502. [[CrossRef](#)]
38. Fang, W.; Xie, H.; Yin, F.; Li, J.; Khan, D.F.; Fang, Q. Molecular dynamics simulation of grain boundary geometry on crack propagation of bi-crystal aluminum. *Mater. Sci. Eng. A* **2016**, *666*, 314–319. [[CrossRef](#)]
39. Thompson, A.P.; Plimpton, S.J.; Mattson, W. General formulation of pressure and stress tensor for arbitrary many-body interaction potentials under periodic boundary conditions. *J. Chem. Phys.* **2009**, *131*, 154107. [[CrossRef](#)]
40. Rycroft, C.H. VORO ++: A three-dimensional Voronoi cell library in C ++. *Chaos* **2009**, *19*, 041111. [[CrossRef](#)] [[PubMed](#)]
41. Stukowski, A.; Bulatov, V.V.; Arsenlis, A. Automated identification and indexing of dislocations in crystal interfaces. *Model. Simul. Mater. Sci. Eng.* **2012**, *20*, 085007. [[CrossRef](#)]
42. Stukowski, A. Visualization and analysis of atomistic simulation data with OVITO—the Open Visualization Tool. *Model. Simul. Mater. Sci. Eng.* **2010**, *18*, 015012. [[CrossRef](#)]
43. Dowling, N. *Mechanical Behavior of Materials*, 4th ed.; Pearson: London, UK, 2012.
44. Velilla-Díaz, W.; Pacheco-Sanjuan, A.; Zambrano, H.R. The role of the grain boundary in the fracture toughness of aluminum bicrystal. *Comput. Mater. Sci.* **2019**, *167*, 34–41. [[CrossRef](#)]
45. Thaulow, C.; Schieffer, S.V.; Vatne, I.R.; Sen, D.; Østby, E. Crack Tip Opening Displacement in atomistic modeling of fracture of silicon. *Comput. Mater. Sci.* **2011**, *50*, 2621–2627. [[CrossRef](#)]
46. Skogsrud, J.; Thaulow, C. Application of CTOD in atomistic modeling of fracture. *Eng. Fract. Mech.* **2015**, *150*, 153–160. [[CrossRef](#)]
47. Skogsrud, J.; Thaulow, C. Effect of crystallographic orientation on nanomechanical modelling of an iron single crystal cracked cantilever beam. *Mater. Sci. Eng. A* **2017**, *685*, 274–283. [[CrossRef](#)]
48. Clatterbuck, D.M.; Krenn, C.R.; Cohen, M.L.; Morris, J.W. Phonon instabilities and the ideal strength of aluminum. *Phys. Rev. Lett.* **2003**, *91*, 135501. [[CrossRef](#)] [[PubMed](#)]